Non-invasive MR thermometry monitoring in plasmonic photothermal therapy using gold nanorods

Seung-Hyun Yang
Yonsei University
Kiyoung Jeong
Yonsei University
Jaemoon Yang
Yonsei University
Hye Young Son
Yonsei University
Jin-Suck Suh
Yonsei University
Yong-Min Huh
Yonsei University
Seung Jae Oh (issac@yuhs.ac)
Yonsei University

Article

Keywords: plasmonic photothermal therapy, gold nanorods, MRI, MR thermometer, tumor phantom

Posted Date: May 19th, 2022

DOI: https://doi.org/10.21203/rs.3.rs-1644381/v1

Abstract

This study used magnetic resonance (MR) thermometry to investigate the temperature increases and thermal diffusion that occur during plasmonic photothermal therapy (PTT) with gold nanorods (GNRs). An artificial tumor phantom made of agarose gel containing GNRs was heated by irradiation with an 808 nm laser. The MR thermometer visualized the conditions: a well-localized temperature distribution with suppressed thermal diffusion that depended on laser power and irradiation time. A tumor phantom model was implanted in mice, and MR thermometry evaluated the temperature change in the presence and absence of GNRs and the thermal diffusion into the surrounding tissues. That experiment showed that MR thermometry can be a useful tool for monitoring PTT. These results suggest that MR temperature measurement could help to establish ideal laser irradiation conditions in GNR-mediated PTT, and that it has great potential for visualizing local photothermal induction and evaluating therapeutic effects.

Introduction

Loco-regional thermal ablation of tumors is a conventional local therapy that uses high temperature to induce tumor cell apoptosis or coagulative necrosis. It has many potential benefits over surgery, including lower morbidity, increased preservation of surrounding normal tissues, reduced cost, and shorter hospitalization time.[1,2] The loco-regional thermal ablation techniques that are clinically available are LITT (laser-induced thermal therapy), RFA (radiofrequency ablation), and HIFU (high-intensity focused ultrasound), which use a laser, radio frequency, and ultrasound, respectively, as the heat source. The challenge in using such techniques is to eliminate abnormal tissue without causing damage to the surrounding normal, healthy tissue. Thus, temperature monitoring and complex simulations that determine the intensity, direction, and shape of the thermal source have been conducted to localize the appropriate amount of heat at the target region.[3–5] Despite such careful attention to the target, treatment of tumor tissues that are irregularly scattered or in complicated radial shapes often damages healthy tissues. That problem can be addressed using therapeutic techniques such as target-specific functional nanoparticles, also known as nanoprobes. When surface plasmon resonance occurs on the nanoparticle surfaces under laser irradiation, only the targeted tumor tissue containing the nanoparticles is heated, protecting the normal region from damage regardless of tumor shape or distribution.[6] In this regard, plasmonic photothermal therapy (PTT) has been studied. PTT combines laser therapy and nanoparticle technology to enable tumor-specific heating. Nanoparticles with tumor-specific molecules, such as an antibody or aptamer, enable selective tumor treatment by PTT. Gold nanorods (GNRs) have been widely used in PTT studies. GNRs can support a higher-absorption cross-sectional area of near infrared waves per unit volume than other types of nanoparticles, and they exhibit a much narrower linewidth than spherical nanoparticles at similar resonance frequencies due to their reduced radiation damping effect.[7] In addition, GNRs have been identified as optimal nanoparticles because they can be synthesized in bulk, have broadly tunable plasmon resonance, and allow easy surface modification. Various cancer treatment and imaging studies using GNRs have been conducted.[8–11] Although PTT cancer treatment using GNRs has been quite effective, accurate temperature monitoring around the GNRs is required to minimize

unintended effects on nearby normal cells. Many studies have been performed to monitor the temperature distribution in regions with and without nanoprobes using visible, mid-infrared, terahertz, and magnetic resonance (MR) imaging.[12–16] Among those options, MR thermometers have been spotlighted as a non-invasive, non-depth-limited tool that does not require ionizing radiation, offers excellent anatomical resolution, and is useful in all scan directions.[2] MR thermometers can measure and profile temperature using several methods, including proton resonance frequency, proton density, magnetization transfer, and diffusion coefficient.[17–19] They are suitable for LITT and PTT applications because they do not interfere with the laser. Even with HIFU, MRI-compatible multi-element ultrasound transducers can be used to provide spatial control of the heating zone.[2] RFA is not recommended with MR thermometry unless proper filtering is implemented because interference between the RF and MR systems is a serious concern.[20] Although it is important to understand the diffusion temperature trends around the tumor, previous MR thermometry studies in PTT have mostly used spherical gold nanoparticles; no previous studies have used GNRs.[21,22] Accurate temperature monitoring studies are needed because GNRs can absorb 3–5 times more light energy from plasmon resonance than spherical gold nanoparticles at the same gold mass.[23] This study used MR thermometry to measure the photothermally induced temperature distribution in a GNR-implanted tumor phantom and a tumor phantom–implanted mouse model. The contours of each temperature distribution within specially selected ranges in the tumor phantom are displayed as binary temperature maps. Analysis of those binary temperature maps shows that MR thermometry can be used to optimize laser irradiation conditions. The temperature distribution and thermal diffusion of the GNR-implanted tumor phantoms were verified *in vivo* using MR thermometry in mice with implanted tumor phantoms. Those experiments confirmed the different tendencies of temperature increases and decreases depending on the presence or absence of GNRs and showed that it is possible to monitor differences in the degree of heat diffusion into surrounding tissue. These results demonstrate that MR thermometry has potential as a monitoring system to confirm the therapeutic effect of PTT and minimize the side effects to normal tissue.

Materials And Methods

Materials

Hexadecyltrimethylammonium bromide solution, sodium borohydride solution, gold(III) chloride trihydrate, ascorbic acid solution, and silver nitrate solution were purchased from Sigma-Aldrich (MO, USA). Agarose powder was purchased from Gendepot (TX, USA). Ultrapure deionized water was used for all syntheses. All other chemicals and reagents were analytical grade.

Preparation of GNR-implanted tumor phantom

GNRs with surface plasmon resonance waves of 808 nm in water were synthesized using a seed-mediated growth technique in a previously published protocol with some modifications.[24] The 50 μM GNRs were included in a cylindrical tumor phantom with a height of 1 cm and diameter of 8 mm that was

located more than 2 mm from the top of a rectangular phantom. A 2-mm layer of agarose covered the top surface of the phantom, as shown in Fig. 1.

Laser irradiation

Throughout the experiments, laser irradiation was implemented at a room temperature of ~ 20°C.[25] A continuous wave laser beam of 808 nm was guided to the phantom via a 10-m optical fiber, as shown in Fig. 1. The laser irradiation had a diameter of 10 mm, larger than the tumor phantom size, with power densities of 3.8 W/cm^2 and 6.4 W/cm^2.

MR thermometry

Throughout the experiments, MR thermometry was implemented at a room temperature of ~ 20°C. The MR signals of the tumor phantom were obtained using an 8ch HD T/R hand coil (GE Healthcare, IL, USA). Images for the thermo map were acquired by fast spoiled gradient echo pulse sequence on a 3.0 T GE Discovery MR750 scanner. The parameters were TR/TE = 3500/79.6, image matrix = 256 × 256, slice thickness = 4 mm. The acquisition time per slide was approximately 10 seconds, and 6 and 24 slides were obtained before and after laser irradiation, respectively. The proton resonance frequency method was used to reconstruct the temperature maps, and the algorithm was executed by IDL (Version 8.2, Exelis Visual Information Solutions, Inc., VA, USA). The temperature map was analyzed considering the specific temperature boundaries inside and outside the phantom.

Animal care and in vivo *MR thermometry*

Five-week-old male athymic BALB/c nude mice (Orient Bio, Korea) were used for the tumor phantom experiments. The mice were retained in microisolator cages under sterile conditions and observed for at least 1 week before study initiation to ensure their proper health. Temperature, lighting, and humidity were controlled centrally. All experimental procedures were carried out in accordance with the guidelines of the Institutional Animal Care and Use Committee and approved by Yonsei University College of Medicine. Before the experiments, all mice were anesthetized with 2% isoflurane. Tumor phantoms mixed with Matrigel® matrix (Corning, AZ, USA) and 50 μM GNRs were prepared and transplanted onto the left thigh of each mouse. For the control group, only Matrigel was transplanted without GNRs. After the Matrigel was sufficiently hardened by mouse body temperature, MR thermometry was performed during laser irradiation. The MR thermometry measured the temperature every 10 seconds, and the laser irradiation lasted 250 seconds.

Results

Temperature mapping after laser irradiation

To confirm the non-invasive temperature measurement capability of MR thermometry, tumor phantoms with and without GNRs were prepared using agarose gel and were irradiated with a laser, and then the

temperature inside each tumor phantom was measured using MR thermometry. Figures 2A and B show the T2 MR images of the tumor-mimicking phantoms with and without GNRs before laser irradiation. When a laser beam with 6.4 W/cm^2 of power was used for 140 seconds on both phantoms, the conventional T2 MR images of the GNR phantom and GNR-free phantom did not differ significantly. However, when image reconstruction for temperature was applied, a significant temperature difference was clear, as shown in Figs. 2C and D. The maximum temperature increase for the GNR-implanted tumor phantom was 16°C, whereas the tumor phantom without GNRs experienced only a very slight temperature increase due to the laser irradiation itself. As shown in Fig. 2F, in the tumor phantoms with GNRs, thermal diffusion was observed from the center to the outside unlike Fig. 2E tumor phantom without GNRs.

Characterization of heat diffusion profiles

Ideally, PTT increases the temperature of the target area as much as intended and prevents thermal damage in the surrounding area by suppressing temperature changes there. Therefore, the boundary of each temperature range must be carefully monitored during heat diffusion in both the normal and abnormal regions. Because the effectiveness of PTT is highly dependent on thermal dose,[25] various temperatures were used as guidelines, and a binary temperature contour map was applied to characterize the temperature and thermal diffusion around the tumor phantom. Figure 3A shows the changes in areas of the GNR-implanted tumor phantom in which the temperature increased by 6, 8, and 10°C upon irradiation with a 3.8 W/cm^2 laser. After 80 seconds of laser irradiation, most areas of the tumor phantom had increased by 6°C but had not been affected to the extent to increase the temperature by 8 or 10°C. After 300 seconds, the heat increase was in the 6 and 8°C range. Figure 3B shows the results from irradiation with a 6.4 W/cm^2 laser. Most of the tumor phantom had increased by 10°C in 80 seconds. The area that increased by 14°C was very wide, and the 6°C increase had begun to affect the surrounding area. The area with a 6°C increase was much larger than the tumor phantom after 300 seconds, but the area with a 14°C increase remained well localized in the phantom, with no significant change from 80 seconds. These results show that laser power and irradiation time should vary depending on the temperature increase needed in the irradiation site, and that MR thermometry monitoring is an important tool for controlling heat diffusion into normal tissues.

Assessment of heat localization efficiency

To evaluate the localization efficiency of various temperature ranges according to laser power and exposure time, the tumor phantom area was divided into 4 areas, as shown in Fig. 4A: all regions in which the temperature increased (area 1), the regions with a temperature increase that corresponded to the tumor phantom (area 2), the regions outside the tumor phantom with a temperature increase (area 3), and the tumor phantom regions in which the temperature did not increase (area 4). Areas 1 and 2 expanded over time during laser irradiation, but it was predicted that there would be no further change once area 2 was equal in size to the area of the tumor phantom. The temperature in area 3, outside the tumor phantom, should increase after that in all other tested areas. At the start of the experiment, area 4 was the

same as the tumor phantom, and it was expected to decrease during laser irradiation. Therefore, the optimal treatment condition, in which heat is concentrated in the tumor site and diffusion to the periphery is suppressed, would show similar increases in areas 1 and 2 and approaching contact of graphs of areas 3 and 4 during laser irradiation. With laser irradiation at 3.8 W/cm^2, the areas in which the temperature increased by 6 and 8°C were wider than the tumor phantom, and there was heat diffusion to the outer area (Fig. 4B). On the other hand, the area in which the temperature increased by 10°C was localized to the tumor phantom and remained nearly identical to areas 1 and 2. After 110 seconds of laser irradiation, areas 1 and 2 stopped showing significant changes, and areas 3 and 4 contacted each other. Thus, if a tumor is treated using the same conditions as the tumor phantom, laser irradiation of 110 seconds or more is required to increase the temperature by 10°C. With the 6.4 W/cm^2 laser, thermal diffusion occurred in both the 6 and 10°C increase regions, which were wider than the 6 and 8°C increase regions with 3.8 W/cm^2 laser irradiation. On the other hand, the area with a 14°C increase remained well localized to the tumor phantom. The initial laser irradiation produced increases that almost matched those of areas 1 and 2. After 100 seconds of laser irradiation, areas 1 and 2 no longer showed significant changes; areas 3 and 4 contacted each other after 140 seconds of laser irradiation. Unlike the other conditions, the increase in area 3 was greatly suppressed. The MR thermometry showed that the 14°C increase was well localized to the tumor phantom area under irradiation from a 6.8 W/cm^2 laser, and heat diffusion to the periphery was suppressed (Fig. 4C). These MR thermometry results show that thermal diffusion differs widely depending on set temperature and laser power. They also suggest that MR thermometry is a useful tool for monitoring these phenomena.

In vivo *MR thermometry*

To use MR thermometry to evaluate the temperatures, changes, and thermal diffusion according to presence of GNRs and laser irradiation *in vivo*, a mouse experiment was conducted. Tumor phantoms were implanted in the left thighs of mice using Matrigel®, and the internal temperature change caused by laser irradiation was measured with MR thermometry (Fig. 5A). In the tumor phantoms with GNRs, the temperature increased rapidly after 50 seconds of laser irradiation but was concentrated in the GNR region (Fig. 5B). In the control tumor phantom, laser irradiation generated only weak heat that spread widely to the surrounding area. The control tumor phantom showed no significant temperature change for about 50 seconds after the start of laser irradiation, and then the temperature changed slowly to a maximum increase of 12.64°C until the laser was turned off. The GNR-implanted tumor phantom increased rapidly in temperature after the start of laser irradiation, increased by 12.59°C in 50 seconds, and then continued to a maximum increase of 26.19°C until the laser was turned off. After turning off the laser, the temperature of the tumor phantom containing the GNRs decreased rapidly and was only 3.08°C higher than the starting temperature after 700 seconds. In the control tumor phantom, on the other hand, the temperature decreased slowly even after the laser was turned off, and the temperature after 700 seconds was 7.94°C above starting temperature (Fig. 5C). These results demonstrate that MR thermometry can precisely monitor heating of the target site and diffusion of heat to the periphery of PTT

using GNRs. It also suggests that MR thermometry is a useful tool for preventing unintended side effects in normal tissues.

Discussion

In PTT, monitoring the temperature and thermal diffusion of the laser site is important to ensure treatment effectiveness and to reduce side effects. MRI is a non-invasive imaging technique that can acquire anatomical images without depth limitation and can be applied to precisely measure temperature change, location, and thermal diffusion of PTT. A tumor phantom of agarose gel and GNRs was placed in an MRI machine and irradiated with a laser. A binary temperature map was applied at specific temperatures to evaluate changes in appropriate heat locations and diffusion according to laser irradiation time and output. Areas with an increase of 6 or 8°C showed rapid heat diffusion into the surrounding tissue, even with low-power laser irradiation. The temperature maps show that the 10 and 14°C increases occurred predominantly at the tumor phantom location, and heat diffusion to the surroundings was suppressed. These results suggest that it is necessary to precisely control the laser power and time according to the required range and temperature when using PTT with GNRs, and that MR thermometry can be useful in that process. In a murine *in vivo* experiment, non-invasive MR thermometry clearly confirmed the thermal diffusion and temperature changes not only in the laser irradiated area, but also in the surrounding areas. MR thermometry made it possible to accurately and conveniently monitor the temperature increase rate, maximum temperature, and thermal diffusion in the presence and absence of GNRs in the tumor phantom. To perform effective PTT, it is important to consider the temperature of the heat source and the environment surrounding the tumor, and MR thermometry is an excellent way to monitor the temperature inside and outside the tumor. In PTT, MR thermometry can be an excellent tool to acquire treatment and diagnosis data simultaneously, suggesting its potential applications in various heat-based therapies.

Declarations

Financial & competing interests

This study was supported by a National Research Foundation of Korea grant funded by the Korean government (NRF-2021R1A6A3A01086846 and NRF-2019M3A6B3030644). The authors have no other relevant affiliations or financial involvement with any organization or entity with a financial interest in or financial conflict with the subject matter or materials discussed in the manuscript.

Submission declaration and verification

The authors declare that this manuscript is original, has not been published before, and is not currently being considered for publication elsewhere.

Author contributions

Seung-Hyun Yang conceived of this work, carried out the experiments, and wrote the manuscript. KiYoung Joung provided technical support during all animal experiments. Jaemoon Yang, Hye Young Son, and Jin-Suck Suh analyzed the MRI data. Yong-Min Huh and Seung-Jae Oh supervised the entire project, were involved in designing all experiments, and revised the manuscript. All authors read and approved the final manuscript.

Additional information

The datasets used and/or analysed during the current study available from the corresponding author on reasonable request.

References

1. Chu KF, Dupuy DE. Thermal ablation of tumours: biological mechanisms and advances in therapy. Nature reviews Cancer. Mar 2014;14(3):199–208. doi:10.1038/nrc3672
2. Rieke V, Butts Pauly K. MR thermometry. Journal of magnetic resonance imaging: JMRI. Feb 2008;27(2):376–90. doi:10.1002/jmri.21265
3. Jolesz FA. *Intraoperative imaging and image-guided therapy*. Springer; 2014:xvii, 893 pages.
4. Goldberg SN, Gazelle GS, Mueller PR. Thermal ablation therapy for focal malignancy: a unified approach to underlying principles, techniques, and diagnostic imaging guidance. AJR American journal of roentgenology. Feb 2000;174(2):323–31. doi:10.2214/ajr.174.2.1740323
5. Gupta PK, Singh J, Rai KN. A numerical study on heat transfer in tissues during hyperthermia. *Mathematical and Computer Modelling*. 2013/ 03/01 / 2013;57(5):1018–1037. doi:https://doi.org/10.1016/j.mcm.2011.12.050
6. Lim EK, Kim T, Paik S, Haam S, Huh YM, Lee K. Nanomaterials for theranostics: recent advances and future challenges. Chemical reviews. Jan 14 2015;115(1):327–94. doi:10.1021/cr300213b
7. Sönnichsen C, Franzl T, Wilk T, et al. Drastic reduction of plasmon damping in gold nanorods. Phys Rev Lett. Feb 18 2002;88(7):077402. doi:10.1103/PhysRevLett.88.077402
8. Huff TB, Tong L, Zhao Y, Hansen MN, Cheng J-X, Wei A. Hyperthermic effects of gold nanorods on tumor cells. Nanomedicine (Lond). 2007;2(1):125–132. doi:10.2217/17435889.2.1.125
9. Schuh EM, Portela R, Gardner HL, Schoen C, London CA. Safety and efficacy of targeted hyperthermia treatment utilizing gold nanorod therapy in spontaneous canine neoplasia. BMC Vet Res. 2017;13(1):294–294. doi:10.1186/s12917-017-1209-y
10. Hauck TS, Jennings TL, Yatsenko T, Kumaradas JC, Chan WCW. Enhancing the Toxicity of Cancer Chemotherapeutics with Gold Nanorod Hyperthermia. Advanced Materials. 2008;20(20):3832–3838. doi:https://doi.org/10.1002/adma.200800921

11. Choi J, Park Y, Choi EB, et al. Aptamer-conjugated gold nanorod for photothermal ablation of epidermal growth factor receptor-overexpressed epithelial cancer. J Biomed Opt. May 2014;19(5):051203. doi:10.1117/1.jbo.19.5.051203
12. Gobin AM, Lee MH, Halas NJ, James WD, Drezek RA, West JL. Near-Infrared Resonant Nanoshells for Combined Optical Imaging and Photothermal Cancer Therapy. *Nano Letters*. 2007/07/01 2007;7(7):1929–1934. doi:10.1021/nl070610y
13. West CL, Doughty ACV, Liu K, Chen WR. Monitoring tissue temperature during photothermal therapy for cancer. J BioX Res. 2019;2(4):159–168. doi:10.1097/jbr.0000000000000050
14. Chen Y, Gnyawali S, Wu F, et al. Magnetic resonance imaging guidance for laser photothermal therapy. Journal of Biomedical Optics. 2008;13(4):044033.
15. Meng X, Zhang B, Yi Y, et al. Accurate and Real-Time Temperature Monitoring during MR Imaging Guided PTT. *Nano Letters*. 2020 /04/08 2020;20(4):2522–2529. doi:10.1021/acs.nanolett.9b05267
16. Oh SJ, Kang J, Maeng I, et al. Nanoparticle-enabled terahertz imaging for cancer diagnosis. *Opt Express*. 2009 /03/02 2009;17(5):3469–3475. doi:10.1364/OE.17.003469
17. MacFall J, Prescott DM, Fullar E, Samulski TV. Temperature dependence of canine brain tissue diffusion coefficient measured in vivo with magnetic resonance echo-planar imaging. International journal of hyperthermia: the official journal of European Society for Hyperthermic Oncology, *North American Hyperthermia Group*. Jan-Feb 1995;11(1):73–86. doi:10.3109/02656739509004949
18. Kägebein U, Speck O, Wacker F, Hensen B. Motion Correction in Proton Resonance Frequency-based Thermometry in the Liver. Top Magn Reson Imaging. Feb 2018;27(1):53–61. doi:10.1097/rmr.0000000000000157
19. Quesson B, de Zwart JA, Moonen CT. Magnetic resonance temperature imaging for guidance of thermotherapy. Journal of magnetic resonance imaging: JMRI. Oct 2000;12(4):525–33. doi:10.1002/1522-2586(200010)12:4<525::aid-jmri3>3.0.co;2-v
20. Vigen KK, Jarrard J, Rieke V, Frisoli J, Daniel BL, Butts Pauly K. In vivo porcine liver radiofrequency ablation with simultaneous MR temperature imaging. Journal of magnetic resonance imaging: JMRI. Apr 2006;23(4):578–84. doi:10.1002/jmri.20528
21. Farashahi A, Zare-Sadeghi A, Shakeri-Zadeh A, et al. Real-time mapping of heat generation and distribution in a laser irradiated agar phantom loaded with gold nanoparticles using MR temperature imaging. *Photodiagnosis and Photodynamic Therapy*. 2019/03/01/ 2019;25:66–73. doi:https://doi.org/10.1016/j.pdpdt.2018.11.010
22. Asadi M, Beik J, Hashemian R, et al. MRI-based numerical modeling strategy for simulation and treatment planning of nanoparticle-assisted photothermal therapy. Physica medica: PM : an international journal devoted to the applications of physics to medicine and biology : official journal

of the Italian Association of Biomedical Physics (AIFB). Oct 2019;66:124–132. doi:10.1016/j.ejmp.2019.10.002

23. Baffou G, Quidant R, Girard C. Heat generation in plasmonic nanostructures: Influence of morphology. Applied Physics Letters. 2009;94(15):153109.
24. Hong Y, Lee E, Choi J, et al. Gold Nanorod-Mediated Photothermal Modulation for Localized Ablation of Cancer Cells. Journal of Nanomaterials. 2012/10/16 2012;2012:825060. doi:10.1155/2012/825060
25. Mertyna P, Dewhirst MW, Halpern E, Goldberg W, Nahum Goldberg S. Radiofrequency ablation: The effect of distance and baseline temperature on thermal dose required for coagulation. International Journal of Hyperthermia. 2008/01/01 2008;24(7):550–559. doi:10.1080/02656730802035662

Figures

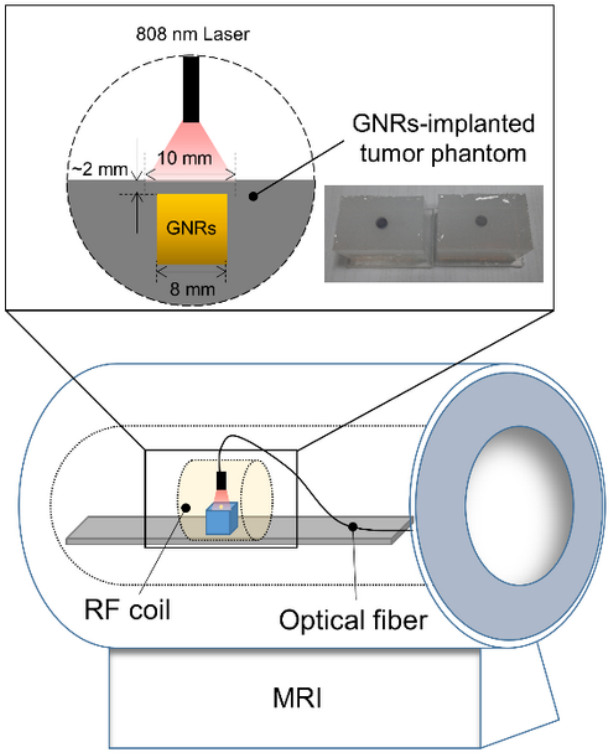

Figure 1

Schematic image of the experiments.

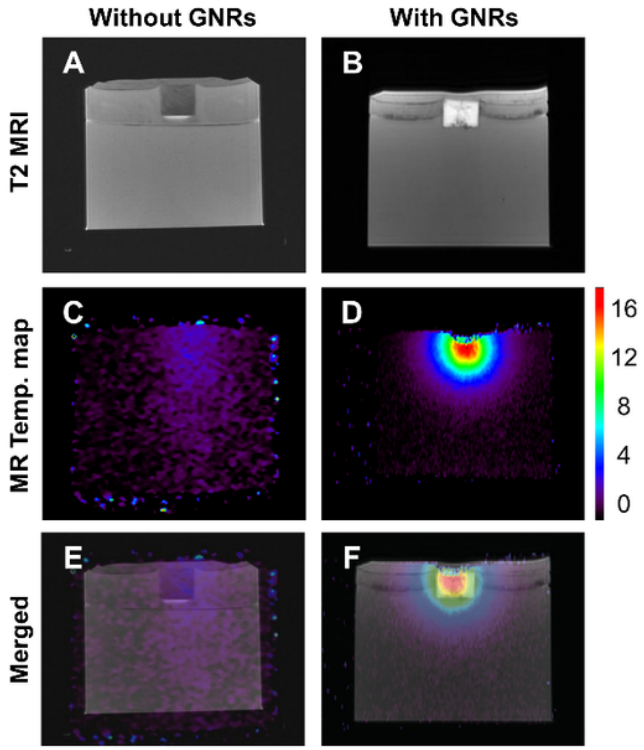

Figure 2

MR images and temperature map of the tumor phantoms. (A) and (B) T2 MR images of the tumor phantoms, (C) and (D) temperature maps of the tumor phantoms after laser irradiation, (E) and (F) merged images of the tumor phantoms. The color bar scale is temperature difference (°C).

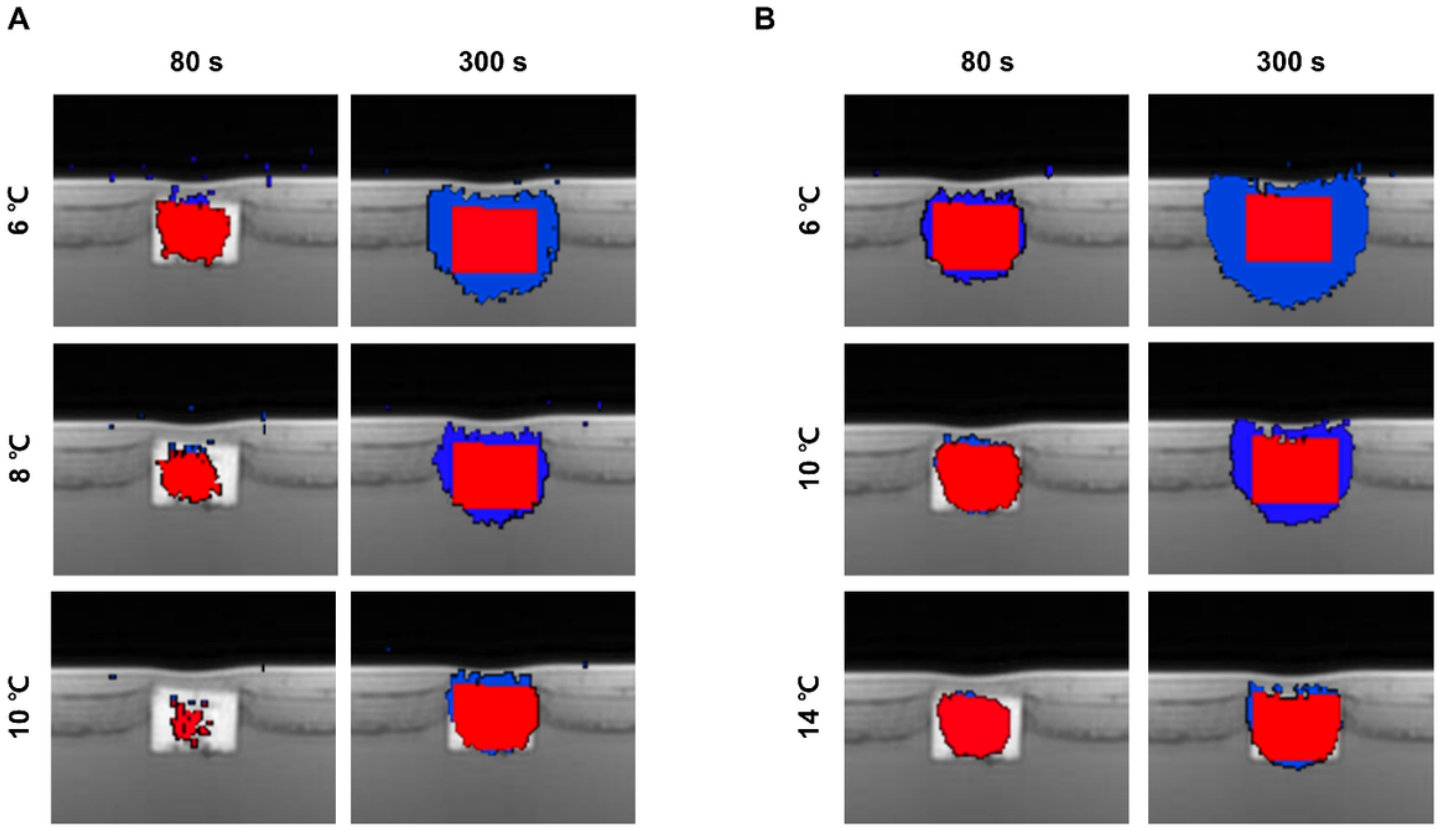

Figure 3

MR thermometry of tumor phantoms with GNRs during laser irradiation. For each area, increases of 6, 8, and 10 °C were measured upon 3.8 W/cm^2 laser irradiation (A), and 6, 10, and 14 °C increases were measured upon 6.4 W/cm^2 laser irradiation (B).

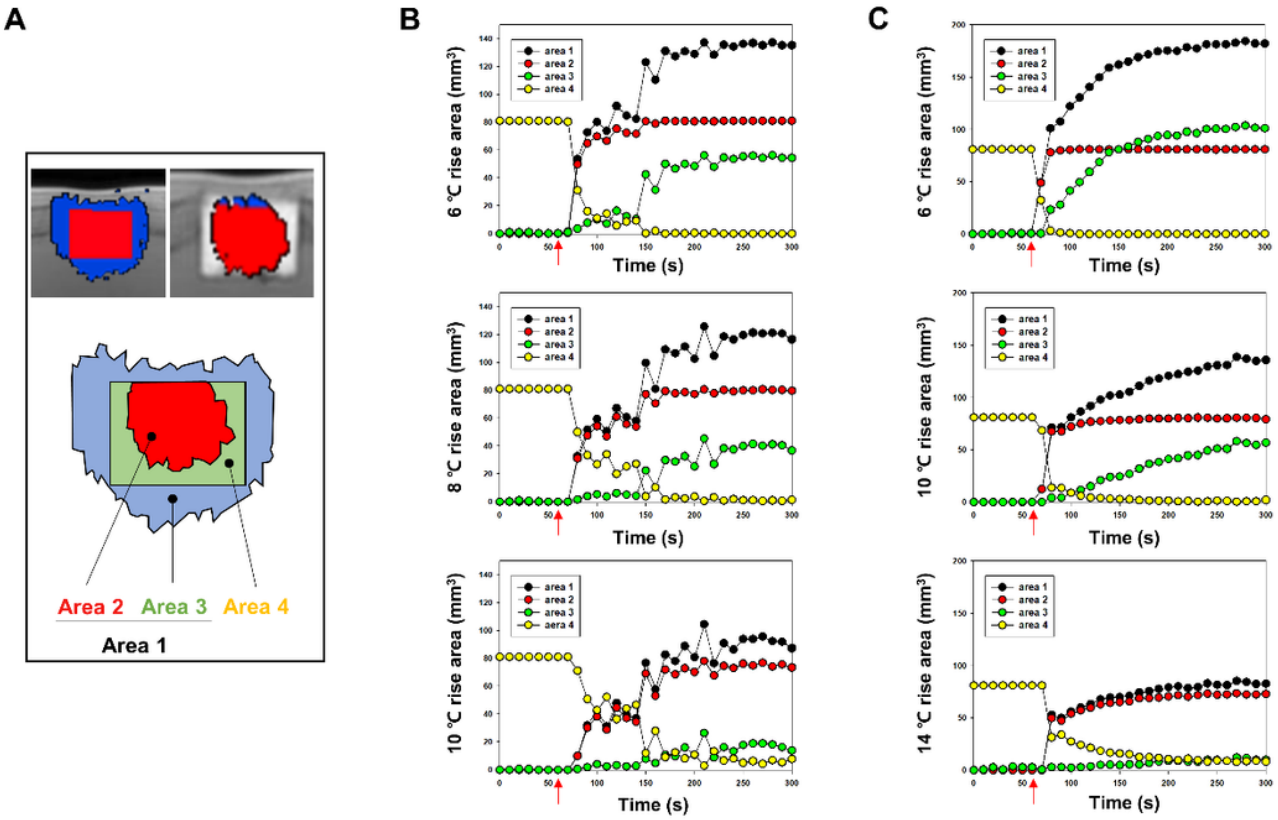

Figure 4

Heat localization graph at various temperatures. The experimental area was divided into 4 regions (A). Areas increased by 6, 8, and 10 °C were measured upon 3.8 W/cm^2 laser irradiation (B). Areas increased by 6, 10, and 14 °C were measured upon 6.4 W/cm^2 laser irradiation (C). (Red arrow: laser irradiation onset)

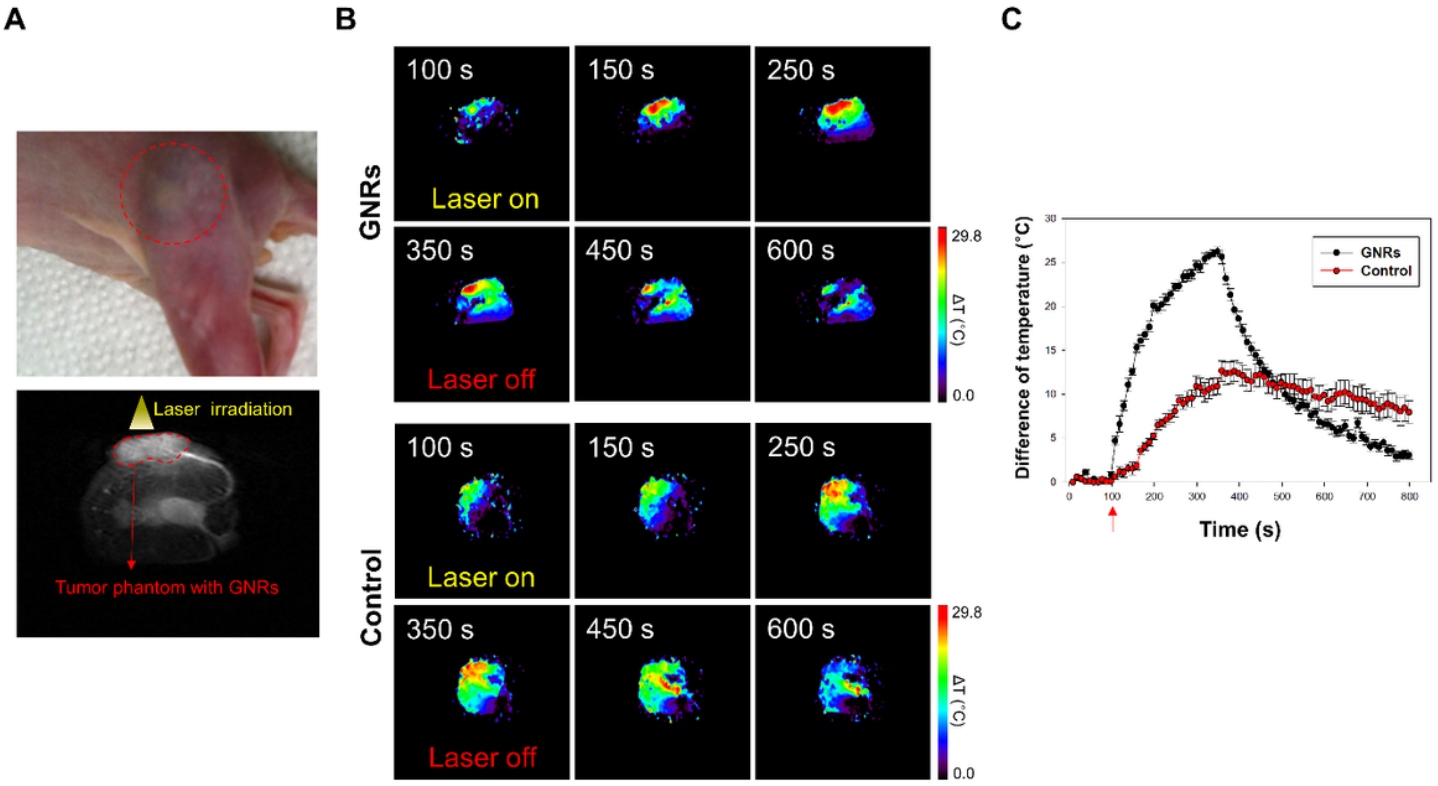

Figure 5

Temperature changes in mouse tumor phantoms upon laser irradiation, measured using MR thermometry. Photo and T2 MR image of mouse tumor phantom (A), MR thermometry upon 16 W/cm^2 laser irradiation (B), and a temperature difference graph of mouse tumor phantoms over time (C). The color bar is temperature difference. (Red arrow: laser irradiation onset)